Masaharu Toyoda received the ME degree in Electrical and Electronic Engineering from Gifu University, Japan, in 2007. He works now in Sony EMCS Corp.

Shin Yabukami received the DE degree in Electrical Engineering from Tohoku University, Japan, in 1998. He is an associate professor in the Department of Electrical Engineering and Information Technology, Tohoku Gakuin University. His research interests are in the area of magnetic sensor, and applied magnetics.

Kasuzhi Ishiyama received the PhD degree in Electrical Engineering from Tohoku University, Japan, in 1993. He is a professor in the Research Institute of Electrical Communication, Tohoku University. His research interests are in the area of magnetic actuators, and magnetic materials.

Yasuo Okazaki received the PhD degree from Tohoku University, Japan, in 1993. He is a professor in the Department of Materials Science and Technology, Gifu University. His research interests are in the area of magnetic shielding, and magnetic materials.

Ken Ichi Arai received the PhD degree in Electrical Engineering from Tohoku University, Japan, in 1971. He is a professor emeritus in Research Institute of Electrical Communication, Tohoku University and an administrator in the Research Institute for Electric and Magnetic Materials. His research interests are in the area of physical properties and application of magnetic materials.

Hiroyasu Kanetaka received the PhD degree in Dentistry from Tohoku University, Japan, in 1997. He is an associate professor in the Center for Research Strategy and Support (CRESS) and Graduate School of Dentistry, Tohoku University. His research interests are in the area of swallowing act.

Interface Oral Health Science 2007: 355–356

Development of a new ultra-precision-polished pure titanium mirror for dental treatment

Hiroyasu Kanetaka*, Akihiro Suzuki, Ryo Tomizuka, Sachiko Urayama, and Teruko Takano-Yamamoto
Division of Orthodontics and Dentofacial Orthopedics, Tohoku University Graduate School of Dentistry, Sendai 980-8575, Japan
*kanetaka@mail.tains.tohoku.ac.jp

Abstract. The aim of this study was to develop a biosafe and a biocompatible mirror for dental treatment. Mirrors are indispensable manual instruments for dental care and are widely used for intraoral examination and treatment. In this study, light and highly biocompatible mirrors were developed by mirror-polishing of pure titanium and used for dental examination and intraoral photography. The surface roughness and reflectance of the dental mirrors were measured and compared with those of commercially available dental mirrors made of stainless steel. Our results suggested that the pure titanium mirror with a mirror-polished surface was satisfactory for clinical use.

Key words. pure titanium, mirror, dental treatment, biocompatibility, polishing

Introduction

Recently, direct-reflection-type metal mirrors with a mirror-polished metal surface have been used because of several advantages, including distinctness of the reflected image, high safety, and improved operability. However, most metal mirrors are made of stainless steel and contain about 10% nickel. Such mirrors may not be suitable for medical use because they can elicit strong allergic reactions [1]. In addition to this biosafety problem, corrosion of stainless steel mirrors can be caused by chloride disinfectants, containing mainly sodium hypochlorite [2]. In this study, light and highly biocompatible mirrors were developed by mirror-polishing of pure titanium, and the surface roughness and reflectance of the new titanium dental mirrors were compared with those of commercially available dental mirrors made of stainless steel.

Material and methods

Newly developed mirror was made of pure titanium (Daido Steel Co., Ltd., Nagoya, Japan), finished by ultra-precision mirror polishing, and used to produce dental mirrors and mirrors for intraoral photography. These mirrors were compared with a commercially available dental mirrors made of stainless steel (metal mirror, YDM Co., Tokyo, Japan). The surface roughness and reflectance of four newly developed dental mirrors were compared with those of four commercially available dental mirrors made of stainless steel. Surface roughness (measurement range: around 360 μm) was measured using a three-dimensional non-contact-type surface

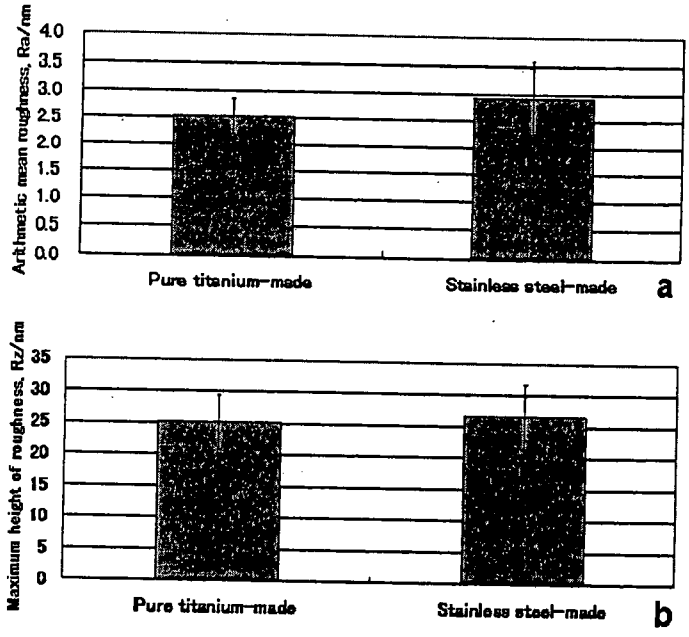

Fig. 1. Surface roughness of metal mirrors

roughness measuring instrument (Talysurf CCI 3000, Taylor Hobson Ltd., Leicester, UK). The reflectance of the mirrors was measured within the visible region (measurement range: 380–780 nm), using a spectrophotometer (U-3120, Hitachi Ltd., Tokyo, Japan). The intraoral mirrors were used to observe teeth and take intraoral photographs.

Results

The arithmetic mean roughness (Ra) of the dental mirror made of pure titanium was 3 nm or less (Fig. 1a), and the maximum height of roughness (Rz) was 30 nm or less (Fig. 1b), comparable to that of the commercially available dental mirror made of stainless steel. Both Ra and Rz showed no significant differences between the two groups.These result suggested that surface of the pure titanium was sufficiently polished by our new original method. The reflectance of the pure titanium mirror was slightly lower than that of the stainless steel mirror, but both provided favorable image.

Conclusion

It was suggested that the pure titanium mirror with mirror-polished surface was considered satisfactory for clinical use.

References

1. Kanerva L, Forstrom L (2001) Allergic nickel and chromate hand dermatitis induced by orthopedic metal implant. Contact Dermatitis 44:103–104
2. Dartar Oztan M, Akman AA, Zaimoglu L, et al (2002) Corrosion rates of stainless-steel files in different irrigating solutions. Int Endod J 35:655–659

Interface Oral Health Science 2007: 181–182

Effects of initially light and gradually increasing force on orthodontic tooth movement

Ryo Tomizuka[1]*, Hiroyasu Kanetaka[1], Yoshinaka Shimizu[2], Akihiro Suzuki[1], Sachiko Urayama[2], and Teruko Takano-Yamamoto[1]

[1]*Division of Orthodontics and Dentofacial Orthopedics;* [2]*Division of Oral and Craniofacial Anatomy, Tohoku University Graduate School of Dentistry, Sendai 980-8575, Japan*

*ryotommy@mail.tains.tohoku.ac.jp

Abstract. This study investigated the effect of initially light and gradual increases in force on tooth movement using the attractive force of magnets in an experimental rat model. The distance between the magnets incrementally decreased from an initial light force in the experimental group, in contrast to no tooth displacement in the control group. There were significant differences in the number of osteoclasts and in the relative hyalinized area on the pressure side of the periodontal tissue between the control group and the experimental group. The application of gradual incremental increases in force induced effective tooth movement in rats, and recruitment of osteoclasts and inhibition of hyalinization.

Key words. initially light force, gradually increasing force, tooth movement, osteoclasts, hyalinization

Introduction

Light continuous force results in a relatively smooth progression of tooth movement by frontal resorption [1]. However, traditional orthodontic appliances are not suitable for generating light force. The objective of this study was to investigate histologically the effect of initially light and gradual increases in force on tooth movement in an experimental rat model.

Material and methods

Sixty male Wistar rats (18 weeks old) were used in the experiment. Cuboids (1.5 mm × 1.5 mm × 0.7 mm) made of magnet (experimental group) or titanium (control group) were bonded on the lingual surface of maxillary first molars. The initial distance between the materials in both groups was 1.5 mm, exerting only a light force in the experimental group. Rats were killed at 1, 3, 7, 10 or 14 days after treatment. Measurement of tooth movement was determined in 28 rats, and the number of TRAP-positive osteoclasts and the relative hyalinized area on the pressure side of periodontal tissue was determined in 32 rats.

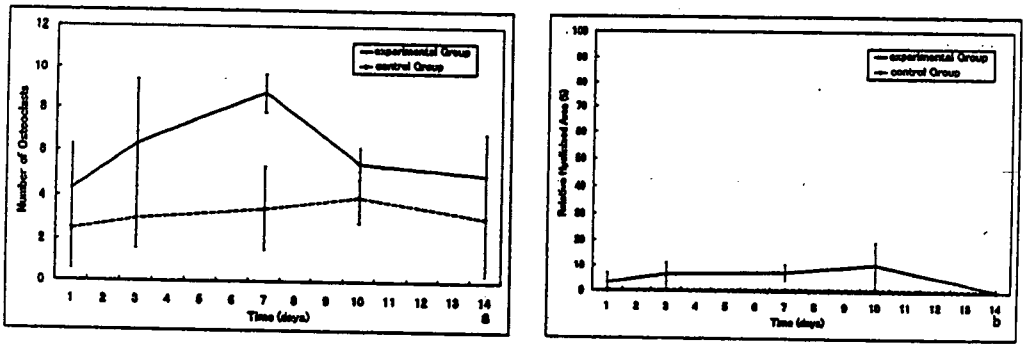

Fig. 1. **a** Time course changes in the number of osteoclasts on the pressure side. **b** Time course changes in the relative hyalinized area on the pressure side

Results and discussion

The distance between the magnets significantly decreased over time in the experimental group, resulting in gradual tooth movement ($P < 0.01$). No tooth displacement occurred in the control group. There was a significant difference in the number of osteoclasts (Fig. 1a) and in the relative hyalinized area between the control group and the experimental group (Fig. 1b) (both $P < 0.01$). We hypothesized that stepwise process may be solved by an application of initially light and gradually increasing force [2]. It is well established that bone resorption by osteoclasts is crucial to orthodontic tooth movement [1, 3]. The formation of resorbed lacunae on the bone surface in the initial stage of force application may be beneficial for the recruitment of osteoclasts and continuous bone resorption, even despite a subsequent increase in force.

Conclusion

The initial application of light force with initially light and gradual increases in force induced effective tooth movement in rats, and recruitment of osteoclasts and inhibition of hyalinization.

References

1. William RP, Henry WF (2000) Contemporary orthodontics, 3rd edn. Mosby, St Louis, pp 296–325
2. Tomizuka R, Kanetaka H, Shimizu Y, et al (2006) Effects of gradually increasing force generated by permanent rare earth magnet for orthodontic tooth movement. Angle Orthod 76:1004–1009
3. Reitan K (1960) Tissue behavior during orthodontic tooth movement. Am J Orthod 46:881–900

Interface Oral Health Science 2007: 329–334

Osteoclast-mediated bone remodeling in guided bone regeneration with sintered bone grafts

Yoshinaka Shimizu[1]*, Keisuke Okayama[1,2], Mitsuhiro Kano[1], Hiroyasu Kanetaka[3], and Masayoshi Kikuchi[1]

[1]*Division of Oral and Craniofacial Anatomy, Department of Oral Function and Morphology;*
[2]*Division of Advanced Prosthodontics, Department of Oral Function and Morphology;*
[3]*Division of Orthodontics and Dentofacial Orthopedics, Department of Oral Health and Development Science, Tohoku University Graduate School of Dentistry, Sendai 980-8575; Japan*
*shimizu@anat.dent.tohoku.ac.jp

Abstract. This study examined the effects of graft material on osteoclast-mediated bone remodeling in guided bone regeneration (GBR). Sintered rabbit bone particles were used as the graft material. A polytetrafluoroethylene membrane was molded into a dome and anchored to the frontal bone in 16 male rabbits. The space under the membrane was filled with a blood clot (control group) or sintered bone particles (experimental group). Animals were killed 2, 4, 8, and 12 weeks after operation. The resected samples were fixed in 4% paraformaldehyde and demineralized. Paraffin-embedded histological sections were stained with hematoxylin and eosin and underwent a histochemical assay to determine tartrate-resistant acid phosphate (TRAP) activity. The proportions of newly formed bone and graft particles and the numbers and densities of osteoclasts and multinucleated giant cells (MGCs) were calculated. The proportion of newly formed bone increased up to 4 weeks in both the control and experimental groups. Subsequently, the proportion decreased in the control group, but did not change significantly in the experimental group. Osteoclast density on newly formed bone was higher in the control group than that in the experimental group. We conclude that the use of a sintered bone graft inhibits bone resorption by osteoclasts.

Key words. guided bone regeneration, sintered bone, bone remodeling, osteoclast, histomorphometry

Introduction

Guided bone regeneration (GBR) has been performed at implant-recipient sites that lack sufficient bone to increase the volume and quality of bone, and thereby enhance implant stability and long-term outcomes. Various devices and surgical techniques have been developed to augment bone. Good clinical outcomes require an understanding of the biologic mechanisms and temporal dynamics of newly formed bone in GBR.

In GBR, bone is newly formed over time in a secluded space containing a blood clot [1]. Initially, woven bone is rapidly formed. This bone is then immediately remodeled to a mature bone with lamellar structure. Although the maintenance of newly formed bone is a prerequisite to creating a biomechanical and clinical environment conducive to long-term implant stability, mature bone gradually decreases in response to various extrinsic factors [2], subsequently entering the marrow spaces [3]. Previous studies have suggested important differences in the pattern of new bone formation in a secluded space containing graft materials [4]. Such materials apparently contribute to the prolonged maintenance of newly formed bone during GBR.

Osteoclasts have important roles in the maintenance and resorption of newly formed bone during bone remodeling. The effects of graft materials on osteoclasts remain unclear. We therefore histomorphometrically investigated the effects of graft materials on the recruitment or localization of osteoclasts and multinucleated giant cells (MGCs) in a model of GBR.

Experimental model of GBR

Sixteen male Japanese white rabbits weighing about 3 kg each were used in this study. General anesthesia was induced by injecting pentobarbital sodium salt (Tokyo Kasei, Tokyo, Japan) at a dose of 0.5 mg/kg body weight into an ear vein. In addition, about 2 ml of local anesthesia (1% lidocaine, Astra Zeneca, Osaka, Japan) was injected subcutaneously into the operation site. The frontal bone was exposed via a midsagittal incision through the skin and periosteum. Cortical bone defects (3×15 mm^2) were made in the external cortical plate of the right and left frontal bones. An expanded polytetrafluoroethylene (e-PTFE) membrane reinforced with a thin titanium mesh (Gore-Tex, WL Gore, AZ, USA) was molded into a dome ($10 \times 5 \times 5$ mm^3) and filled with venous blood from the rabbit's ear in the control group, and sintered bone particles in the experimental group (Fig. 1). Two membranes (control and experimental groups) were placed over the defects and anchored to the bone surface by means of four mini-screws (Ti-SIS pins, SIS-System Trade, Klagenfurt, Austria). The skin was sutured over the membranes.

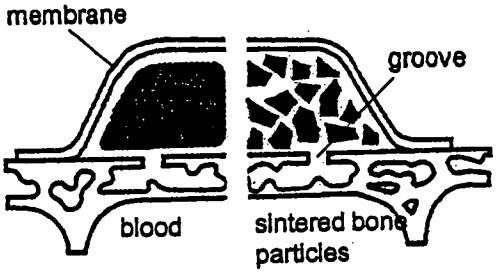

Fig. 1. Schema of the experimental site (frontal section)

Fig. 2. Stereomicroscopic image of pulverized and separated sintered bone particles. *Bar* = 500 μm

Sintered bone particles

The sintered bone particles used in this study were derived from natural rabbit bone. This type of sintered bone is classified as a xenogenic material, with biocompatible and osteoconductive properties [5]. The sintered bone was prepared as follows: boiled rabbit cortical bone was immersed in a mixture of 1% NaOH and 1% H_2O_2 (1:1) to remove proteins on the bone surface for 1 h. The mixture was then neutralized with 1 N HCl. The bone was placed in an electric furnace and sintered at 600°C for 3–5 h and 1,100°C for 3.5 h. The sintered cortical bone was pulverized in a bone mill and sorted into particles of 300–500 μm by means of a standard sieve. The sintered bone particles were white and irregularly shaped on examination with a stereomicroscope (Fig. 2). The calcium and phosphate contents of the sintered bone particles were Ca 42.5%, P 18.2%, and Ca/P ratio 2.34.

Histomorphometry

The rabbits were anesthetized and killed 2, 4, 8, and 12 weeks after operation. For histological examination, the resected samples were demineralized in 10% EDTA and embedded in paraffin. Histological sections were sliced and stained with hematoxylin and eosin and underwent a histochemical assay to determine tartrate-resistant acid phosphate (TRAP) activity. After histological examination by light microscopy, the digitized images were photographed, and the following variables were measured: bone and graft particles volumes, the proportions of bone and graft particles (The bone proportion in the experimental group was calculated as a proportion in the space remaining after exclusion of the graft particles.), and the numbers and the densities of osteoclasts and MGCs. Totally 58 sites of right and left frontal bones in 18 rabbits were used for statistical analyses (two-way analysis of variance and Tukey's test).

Bone formation and sintered bone particles in GBR

Initially, woven bone, lined by a dense layer of cuboidal osteoblasts, proliferated around the groove in the control and experimental groups. The space under the membrane was filled with newly formed bone, fibrous tissue, and adipose tissue at 12 weeks in the control group. Mature bone with a lamellar structure was found from 4 weeks onward. The sintered bone particles were surrounded by newly formed bone, fibrous tissue, and adipose tissue, without inflammatory cell infiltration. The height and extent of newly formed bone were greater in the control group than in the experimental group throughout the experiment (Fig. 3).

Bone volume in the control group increased rapidly for up to 4 weeks ($P < 0.01$) and then decreased significantly ($P < 0.01$). In the experimental group, bone volume increased gradually up to 4 weeks and then did not change significantly. Bone volume in the experimental group was larger than that in the control group from 8 weeks onward (Fig. 4a). The proportion of newly formed bone in the experimental group did not differ from that in the control group at 4 weeks. At 8 and 12 weeks, the proportion of newly formed bone in the experimental group was significantly larger than that in the control group ($P < 0.01$) (Fig. 4b). The proportion of graft particles did not change significantly (Fig. 4c).

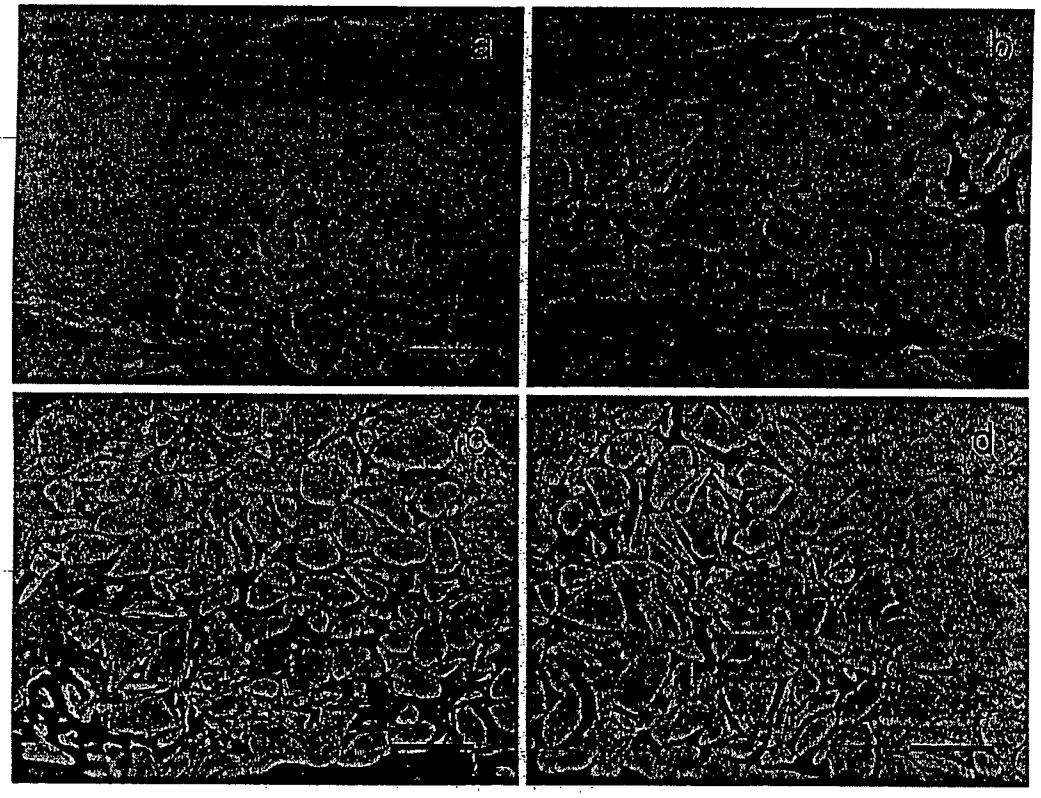

Fig. 3. Histological findings at low magnification (hematoxylin and eosin stain). **a** At 4 weeks in the control group. **b** At 12 weeks in the control group. **c** At 4 weeks in the experimental group. **d** At 12 weeks in the experimental group. *Bars* = 500 μm

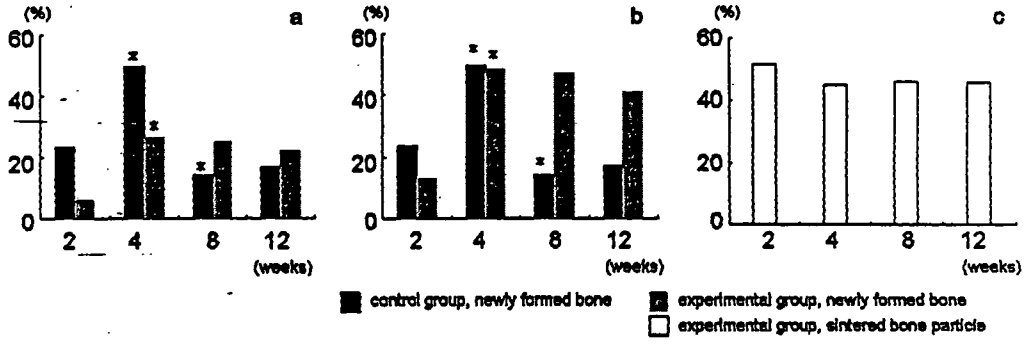

Fig. 4. **a** The volume of newly formed bone. **b** The proportion of newly formed bone in the space remaining after exclusion of the sintered bone particles. **c** The proportion of sintered bone particles. $^{*}P < 0.05$

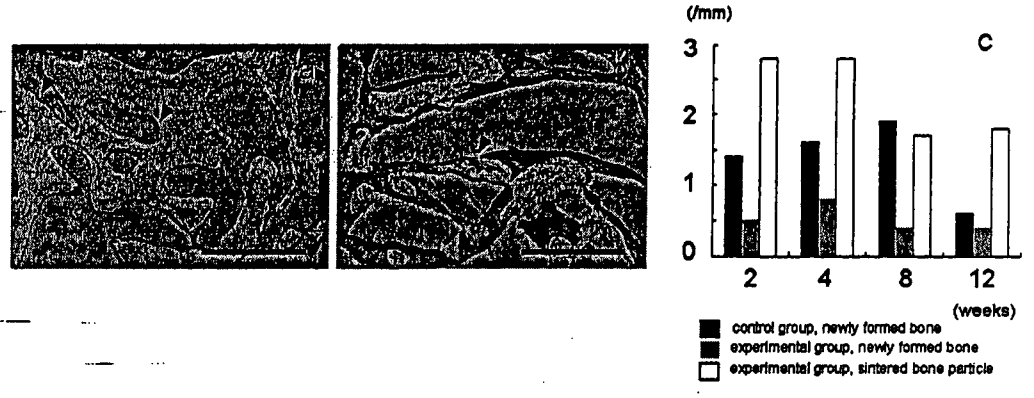

Fig. 5. Histological findings at low magnification (tartrate-resistant acid phosphate). *arrowheads*, osteoclasts or multinucleated giant cells (MGCs). **a** at 4 weeks in the control group. *Bar* = 200 μm **b** at 4 weeks in the experimental group. *Bar* = 200 μm **c** The density of osteoclasts and MGCs

Osteoclasts and multinucleated giant cells in GBR

In both the control and experimental groups, TRAP-positive osteoclasts were found on newly formed bone from 2 weeks onward. At 12 weeks, a few pale osteoclasts were sporadically detected on newly formed bone trabeculae. In the experimental group, TRAP-positive MGCs were detected on the surfaces of sintered bone particles from 2 to 12 weeks (Fig. 5a, b).

The numbers of osteoclasts and MGCs were greatest at 4 weeks in the control and experimental groups. Throughout the experimental period, the number of osteoclasts in the experimental group was lesser than that in the control group. The densities of osteoclasts and MGCs were highest at 8 weeks in the control group and at 4 weeks in the experimental group (Fig. 5c). The densities of osteoclasts and MGCs were lower in the experimental group than in the control group at 2, 4 and 12 weeks. The number of TRAP-positive MGCs increased at 2 weeks and decreased at 8 weeks. The density of TRAP-positive MGCs showed no significant change at 4 weeks and decreased at 8 weeks (Fig. 5c).

Conclusions

Irrespective of the presence or absence of xenografts, the space under the membrane was filled with newly formed bone. In the absence of xenografts, however, newly formed bone decreased gradually in our GBR model. Previous studies have reported that bone is resorbed if it is not functionally stimulated. Bone newly formed at augmented sites may thus decrease at locations not exposed to pressure or tensile stress.

Bone grafts fall into four general categories: autografts, allografts, xenografts, and alloplasts. Sintered bone is classified as a xenograft and considered biocompatible and osteoconductive. Numerous studies of human bone augmentation have shown that bovine-derived particles depleted of organic components are associated with successful bone regeneration. The sintered bone particles had good bone-to-graft contact and showed no change in size for a prolonged period, indicating that this material has nonabsorbable, biocompatible, and osteoconductive properties.

The use of sintered bone particles was associated with no disturbance of bone formation during GBR, but the extension of newly formed bone was delayed. However, the proportion of new bone in the experimental group was equivalent to that in the control group and was maintained. The recruitment of osteoclasts was inhibited, leading to the maintenance of bone volume and proportion. Inhibition of osteoclast activity might be related to the encapsulation of newly formed bone without a foreign body reaction, as well as the transmission of mechanical stress.

A better understanding of the biologic characteristics of new bone in GBR will enable the development of more refined clinical protocols and will facilitate the selection of optimally suited membrane and graft materials. The maintenance of new bone will be achieved by the understanding of bone remodeling, leading to the effective establishment of a functional structure in vivo.

References

1. Nishimura I, Shimizu Y, Ooya K (2004) Effects of cortical bone perforation on experimental guided bone regeneration. Clin Oral Implants Res 15:293–300
2. Asai S, Shimizu Y, Ooya K (2002) Maxillary sinus augmentation model in rabbits: effect of occluded nasal ostium on new bone formation. Clin Oral Implants Res 13:405–409
3. Xu H, Shimizu Y, Onodera K et al (2005) Long-term outcome of augmentation of the maxillary sinus using deproteinized bone particles experimental study in rabbits. Br J Oral Maxillofac Surg 43:40–45
4. Okazaki K, Shimizu Y, Xu H et al (2005) Blood-filled spaces with and without deproteinized bone grafts in guided bone regeneration. A histomorphometric study of the rabbit skull using non-resorbable membrane. Clin Oral Implants Res 16:236–243
5. Matsuda M, Kita S, Takekawa M et al (1995) Scanning electron and light microscopic observations on the healing process after sintered bone implantation in rats. Histol Histopathol 10:673–679

Interface Oral Health Science 2007: 353–354

The effects of orthopedic forces with self-contained SMA appliance on cranial suture in rat

Sachiko Urayama[1]*, Hiroyasu Kanetaka[1], Yoshinaka Shimizu[2], Akihiro Suzuki[1], Ryo Tomizuka[1], and Teruko Takano-Yamamoto[1]
[1]Division of Orthodontics and Dentofacial Orthopedics; [2]Division of Oral and Craniofacial Anatomy, Tohoku University Graduate School of Dentistry, Sendai 980-8575, Japan
*sachiko-u@mail.tains.tohoku.ac.jp

Abstract. This study investigated the effect of orthopedic force applied by shape memory alloy (SMA) wire on the cranial bone growth in efforts to develop a self-contained orthopedic appliance. Expansive forces and compressive forces were applied by Ni–Ti SMA wires to interparietal sutures in Wistar rats. All rats were killed at day 14 or 28 post-treatment. Morphological analyses by soft X-ray and micro-computed tomography, and histological observation were performed. Cranial width in the expansive groups was increased significantly compared to the control group ($P < 0.01$). The increase in cranial width in the compressive groups was inhibited. The results suggest that the self-contained SMA appliance has orthopedic application to the cranium.

Key words. orthopedic force, SMA, morphometrical analysis, rat cranium

Introduction

External orthopedic appliances are frequently applied in clinical orthodontics to modify orofacial growth and to obtain harmonious skeletal relations. Current efforts in the development of orthopedic appliances are aimed at creating new internal appliances that are invisible and are automated so as not to require daily activation [1]. We investigated here the effects of orthopedic forces utilizing shape memory alloy (SMA) wire in a self-contained appliance in an experimental rat model of cranial modification through sutural growth control.

Material and methods

Expansive forces (group A, 50 gf; group B, 150 gf) and compressive forces (group C, 30 gf; group D, 90 gf) were applied to interparietal sutures in Wistar rats (male, 6 weeks old) using Ni–Ti SMA wire (0.018 and 0.014 inch Nitinol classic; 3M Unitek, Monrovia, CA, USA) (Fig. 1a). Two-dimensional morphometric analyses

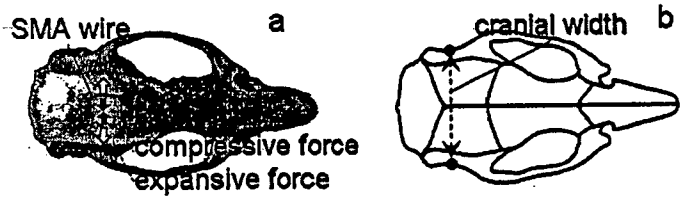

Fig. 1. **a** *SMA wire* applying compressive and expansive forces on the rat cranium. **b** Schema demonstrating the dimension assessed on soft X-ray photographs

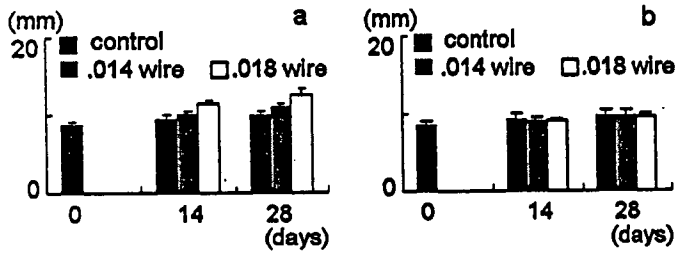

Fig. 2. Time course of cranial width growth in **a** the expansive groups and **b** the compressive groups

to determine cranial width were performed using soft X-ray photographs (Softex, Tokyo, Japan) (Fig. 1b). The interparietal sutures were observed three dimensionally using micro-computed tomography (CT) photographs (ASMX-225CT; Shimadzu Corporation, Kyoto, Japan) and histologically.

Results

Cranial width in the expansive groups was significantly increased compared with the control group ($P < 0.01$, Fig. 2a), whereas cranial width did not significantly differ between the control and compressive groups (Fig. 2b). In the expansive groups, interparietal sutures showed an enlarged opening and thin edges, whereas those in the compressive groups showed a linear shape and thick edges. Three-dimensional observations demonstrated that the interparietal sutures had a more apparent interdigital shape in the expansive groups, compared to a straight form in the compressive groups. Histiologically, new bone formation with osteoblasts on the sutural surfaces was observed in the expansive groups. In contrast, the compressive groups showed osteoclastic resorption and slight hyalinization.

Conclusion

The self-contained orthopedic appliance utilizing SMA wire was found to have orthopedic application to the cranium.

Reference

1. Kanetaka H, Shimizu Y, Hosoda H, et al (2007) Orthodontic tooth movement in rats using Ni-free Ti-based shape memory alloy wire. Mater Trans 48:367–372

J. Magn. Soc. Jpn., 31, 439–444 (2007)

〈Paper〉

Development of a Fingertip Position-Sensing System using LC Resonated Markers

S. Yabukami, K. Ogasawara, H. Saitoh, S. Hashi*, M. Toyoda*, Y. Okazaki*, and K.I. Arai**

Department of Electric and Information Technology, TohokuGakuin University, *1-13-1 Chuo, Tagajo 985-8537, Japan*

*Faculty of Engineering, Gifu University, *1-1 Yanagido, Gifu 501-1193, Japan*

** Research Institute for Electric and Magnetic Materials, *2-1-1 Yagiyama minami, Taihaku-ku, Sendai, 982-0807, Japan*

We propose a new system for sensing the positions of up to five wireless magnetic markers using phase detection. It consists of five resonated markers, a driving coil, and pickup coils. Slim LC resonated markers were fabricated and a detector was formed by connecting high-speed AD converters. The system has a position accuracy of around 1 mm, and can be used for highly accurate position sensing without magnetic shielding, because it is free from earth field noise. We tracked fingertips using five resonated markers.

Key words: wireless LC resonated magnetic marker, position sensing, fingertips

多点ワイヤレス磁気マーカによる指先のモーションキャプチャシステム

薮上 信・小笠原浩太・齋藤秀樹・栃修一郎**・豊田征治**・岡崎靖雄**・荒井賢一***

東北学院大学工学部，多賀城市中央 1-13-1（〒 985-8537）

** 岐阜大学工学部，岐阜市柳戸 1-1（〒 501-1193）

*** 電気磁気材料研究所，仙台市太白区八木山南 2-1-1（〒 982-0807）

1．はじめに

指先の動きは人間らしさを特徴づける運動機能のひとつであり，このモーションキャプチャは人間活動のあらゆる分野・場面へ適用される．キーボード，マウス等は指を用いた最も基本的なインターフェースとして普及している．指先の動きの検出方法には機械式[1]，歪センサを用いる方法[2]，画像処理を用いる方法[3]，交流電磁界を用いる方法[4]等，様々な手法が提案されてきた．しかし日常的に使用可能で，電気的引き出し線やバッテリを持たずに指先の動きを精密に計測可能なシステムは実用化されていない．

筆者らはこれまでマーカへの電気的引き出し線が不要であることと外来ノイズに影響を受けにくいことを両立させることを目指して，共振型の磁気マーカを用いた位置検出システムを提案するとともに，1個のマーカの位置および方向を 1mm 程度の位置精度で検出可能であることを示した[5),6)]．

これまで筆者らが検討してきた磁気マーカによる位置検出システムは複数の磁気マーカを計測する場合でも，それぞれのマーカの共振周波数を異なる値に設定すれば，単一のマーカの位置・方向の検出問題に置き換えることが可能であるため，指先の自然な状態での位置検出に適した方法であると考えた．また本手法は代表的な他の交流磁界を用いる方法[7]に比較して，検出範囲が限定される短所があるものの，指先の動く範囲という比較的限定された範囲であれば，適用可能と考えられる．さらに本手法が有用であれば，上記のマウスやキーボード以外でも指先の運動機能の診断や，障害者の情報入力デバイス等，医療や福祉分野への波及効果も期待できる．

そこで本論文では検出範囲として一辺 150mm 程度の立方体内部を想定し，5個までのワイヤレス磁気マーカの位置および方向をリアルタイムで計測・表示されるシステムを開発した．また5個のマーカを同時にスキャンさせた場合の相対位置精度も議論した．さらに最速 20Hz の計測速度で，マーカを表示可能なシステムを開発した．

2．5個までのマーカの位置・方向の検出方法

Fig. 1 は5個のマーカの位置検出システムを概念的に示

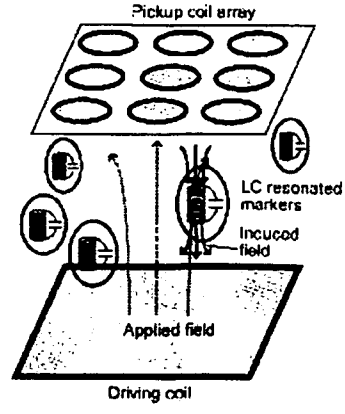

Fig. 1 Schematic diagram of the position-sensing system.

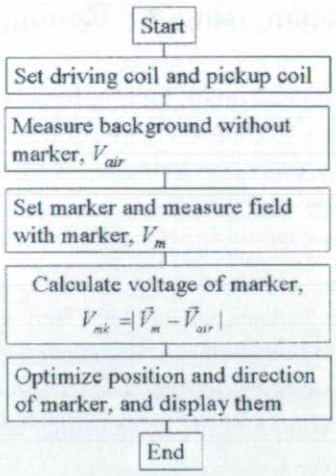

Fig. 2 Flow chart.

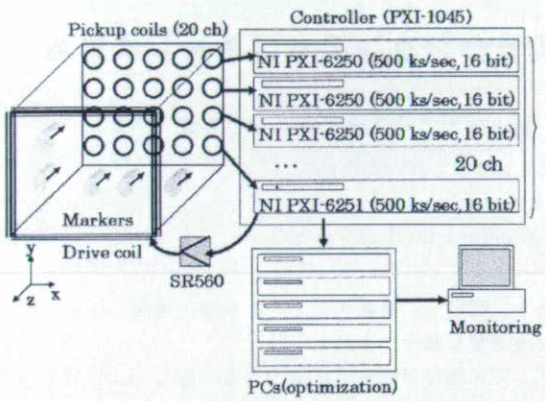

Fig. 3 Schematic diagram of the position-sensing system.

したものであり，励磁コイル，検出コイルおよび磁気マーカから構成される．各々のマーカはインダクタンスとキャパシタンスが接続した等価回路として表した．本システムでは励磁コイルにより各々のマーカの共振周波数における交流磁界を発生させ，マーカからの誘導磁界を検出コイルアレイを用いて計測し，マーカからの誘導磁界をダイポール磁界と仮定してマーカの位置および方向を最適化する．

Fig. 2はマーカの位置および方向を求めるフローチャートを示したものである．まずマーカを取り去った状態で，配置した検出コイルの誘起電圧を測定し，バックグランド電圧とする．次にマーカを配置して検出コイルの誘起電圧を測定する．本稿では各検出コイルの共振周波数においてマーカがない状態での誘起電圧の振幅，マーカをおいた状態での振幅，および両者の電圧の位相差を測定し，ベクトル的に等価的なマーカ寄与電圧を求めた．1個のマーカの共振周波数における磁界分布はそのマーカからの誘導磁界のみであると仮定した．マーカの位置および方向はマーカから発生する誘導磁界がダイポール磁界に近似できることを仮定して，(1)～(3)式により位置および方向をGauss-Newton法[8]により最適化処理する．

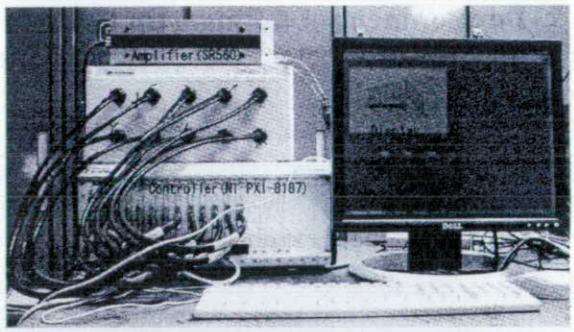

(a) AD converters, amplifier, and display

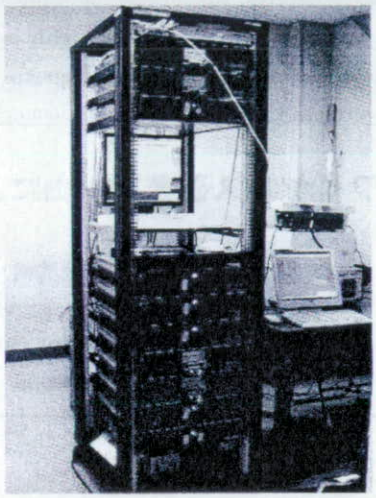

(b) PCs for optimizing the positions of markers

Fig. 4 Photograph of the electrical equipment.

$$S(\vec{p})=\sum_{i=0}^{n}(B_m^{(i)}-B_c^{(i)}(\vec{p}))^2 \tag{1}$$

$$\vec{B}^{(i)}{}_c(\vec{p})=\frac{1}{4\pi\mu_o}\left\{-\frac{\vec{M}}{r_i^3}+\frac{3(\vec{M}\cdot\vec{r}_i)\cdot\vec{r}_i}{r_i^5}\right\} \tag{2}$$

$$\vec{p}=(x,y,z,\theta,\phi,M) \tag{3}$$

ただしSは評価値であり，$\vec{p}$はパラメータベクトルである．iは検出コイルの番号（1～n），$\vec{B}^{(i)}{}_c(\vec{p})$は双極子磁界を考慮した検出コイル$i$における磁束密度の理論値，$\vec{r}$はマーカから検出コイル$i$への位置ベクトル，$\vec{M}$はマーカの磁気モーメント，$(x,y,z)$はマーカ$i$の座標，$\theta$はxy平面へ射影したモーメントの方向ベクトルとx軸とのなす角，ϕはモーメントの方向ベクトルとz軸とのなす角である．Gauss-Newton法の初期値は一つ前のステップにおける収束値を用いた．Gauss-Newton法[8]における縮小因子αは約0.1とした．

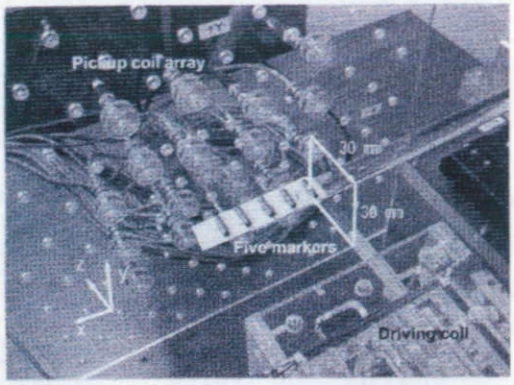

(a) Pickup coil array, driving coil, and five markers

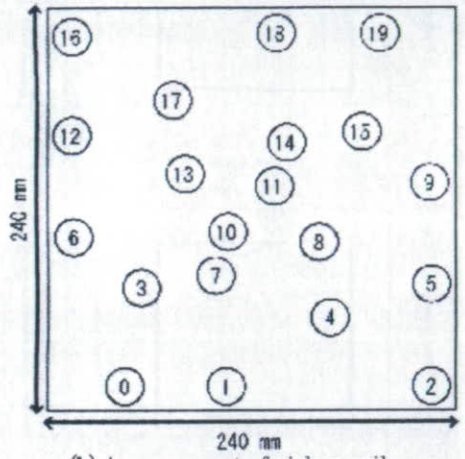

(b) Arrangement of pickup coils

Fig. 5 Arrangement of coils and marker.

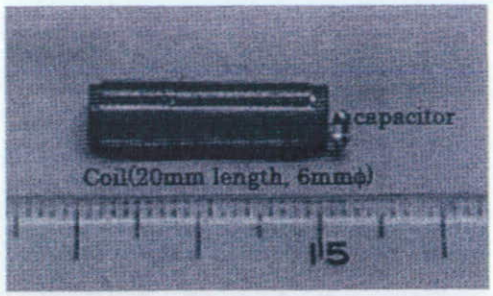

Fig. 6 Photograph of the LC resonated marker.

3. 位置検出システム

Fig. 3は試作した位置検出システムの構成を示したものである．計測システムは励磁コイル，検出コイルアレイ(20チャンネル)，LC共振型磁気マーカ，ADコンバータおよびDAコンバータ（NI PXI-6251：1台），ADコンバータ（NI PXI-6250：9台），制御ユニット（NI PXI-8187），プリアンプ（SR560）から構成される．制御用プログラムはLab VIEW ver. 7.1，位置および方向の最適化処理プログラムはVisual C++を用いて作成した．ADコンバータであるPXI-6251およびPXI-6250は500ksample/secのサンプリング速度で，1台あたり2チャンネルの16ビット信号を計測するモードで使用し，20チャンネルの検出コイルの誘起電圧を並列に取得できるように構成した．励磁コイルへの電圧はPXI-6251からの出力信号をアンプを介して励磁コイルへ接続した．すべてのADコンバータおよびDAコンバータはPXIシステムのため相互に同期が取れており，基準信号に対する位相差を計測可能である．磁気マーカは励磁コイルと検出コイルから構成されるユニット内部に配置した．マーカの位置および方向の最適化処理はイーサネット接続した別のパソコン（Pentium(R)D, 3.20GHz）をマーカの個数台用意して，マーカ位置および方向を並列に演算した．マーカ位置は画面上に表示させた．

Fig. 4(a)は計測システムに用いたPXI制御コントローラ（ADコンバータとDAコンバータを内蔵），プリアンプおよびディスプレイの写真である．Fig. 4(b)はマーカの位置および方向の最適化処理用パソコンである．

Fig. 5は励磁コイル，検出コイル，マーカの写真である．Fig. 5(a)は励磁コイルとマーカ配置を示したものである．励磁コイルおよび検出コイルはアクリルで作成した一辺150mmの立方体に配置し，励磁コイルと検出コイルの面は150mmの距離で対向させた．励磁コイルは一辺約150mmの正方形であり，直径1.0mmの銅線を20ターン施した．Fig. 5(b)は検出コイルの配置を示したものである．検出コイルは線径0.2mmの銅線を直径23mm, 125ターンのコイルに施し，同一平面状に20個配置した．丸枠は実際の検出コイルの寸法を示しており，丸枠内の数値は検出コイルの番号を示している．検出コイルの配置位置は実際に一辺150mmの立方体内部に各指先に5個のマーカを配置して、局所解による影響が十分小さくかつ正確にマーカ位置が検出できるように実験的に決めた．

Fig. 6は試作した磁気マーカのひとつの写真を示したものである．マーカはコイル，コンデンサを半田で直列に接続して作成した．マーカは直径5mm, 長さ20mmのMnZnフェライト（TDK株式会社製EEシリーズ）の周囲に直径0.1mmの銅線を500ターン巻いて外形寸法が長さ20mm，直径約6mmとした．約90kHzにおけるインダクタンスは約5.6mH性能指数は約60であった．コンデンサは0.64nFのチップコンデンサ（ROHM社製MCHシリーズ）を使用した．マーカは非導体による3軸スキャナにより移動させた．

4. 実測結果

4.1 5個のマーカの相対位置精度

5個のマーカの配置および移動はFig. 5(a)の矢印で示したようにマイクロメータにより一辺30mmの正方形を描いた．5個のマーカは1列に並べて，アクリル棒を介して

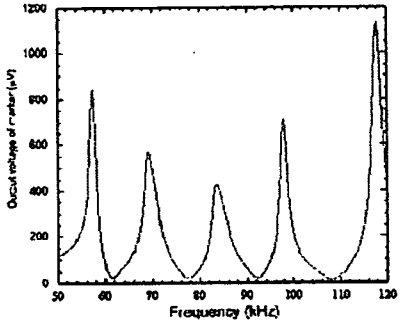

Fig. 7 Frequency of the induced voltage of five markers.

Table 1 Each marker.

	Marker 1	Marker 2	Marker 3	Marker 4	Marker 5
Inductance (mH)	5.6	5.4	5.6	5.1	5.7
Capacitance (nF)	1.3	0.97	0.64	0.52	0.32
Resonant frequency (kHz)	57.5	69.5	83.5	98.0	118.0

Table 2 Position accuracy.

	Marker 1	Marker 2	Marker 3	Marker 4	Marker 5
xy plane	0.5	0.4	0.8	0.2	0.5
yz plane	0.8	0.7	0.5	1.0	1.0
total	0.9	0.8	0.9	1.0	1.1

Unit: mm

接続した，3軸のマイクロメータにより正確に移動させた．近接したマーカ間の距離は約20mmとした．

Fig. 7はマーカの誘導電圧の周波数依存性を示したものである．誘導電圧がピークとなる周波数はそれぞれ57.5 kHz, 69.5 kHz, 83.5 kHz, 98.0 kHz, 118.0kHzであった．Table 1には5個のマーカのインダクタンス，キャパシタンス，共振周波数を示した．本計測システムにおける振幅および位相の計測確度は，測定周期が0.1秒(10Hz)であれば，振幅確度は約1.7 μ V，位相確度は5.1 mdegreeであり，SN比は最大で100程度であった．

Fig. 8はFig. 5(a)に示すように5個のマーカをアクリル棒に固定して同時に移動させた時の各マーカの中心位置を示したものである．それぞれのマーカは約20mmずつ離して配置した．マーカはFig. 5(a)のyz平面内で30mm × 30mmの正方形にマイクロメータを用いて移動させた．30mm × 30mmの移動距離は指の動きの範囲を目安として設定した．最も左に配置したマーカをmarker1とし，隣接する順にmarker2, marker3, marker4, marker5とした．Fig. 8(a)はmarker1の軌跡を表し，Fig. 8(b), Fig. 8(c), Fig. 8(d), Fig. 8(e)はそれぞれmarker2, marker3, marker4, marker5の軌跡を表している．各軌跡はyz平面およびxy平面への射影をそれぞれ示した．計測周期は10Hzとした．●はシステムによって得られたマーカの中心位置であり，実線は理論値を示している．マイクロメータの移動方向とシステムのxyz軸は一致していないため，yz平面への軌跡の射影は若干平行四辺形になり，xy平面への射影は理想的な直線からはずれている．理論値は一辺30mmの正方形を実測された平行四辺形に近い軌跡と

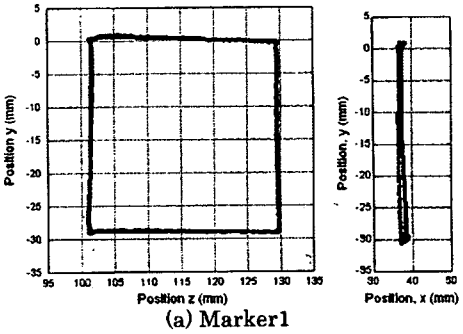

(a) Marker1

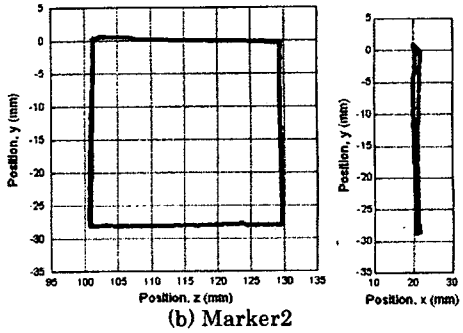

(b) Marker2

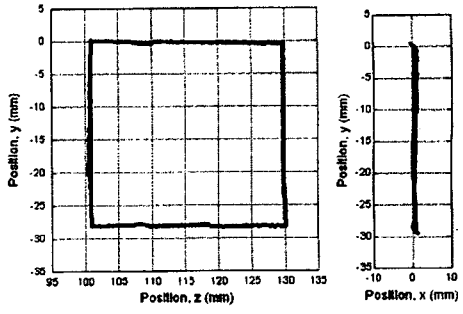

(c) Marker3

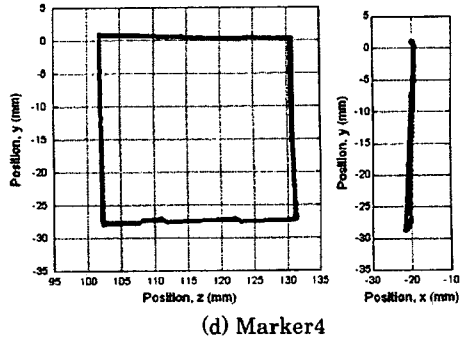

(d) Marker4

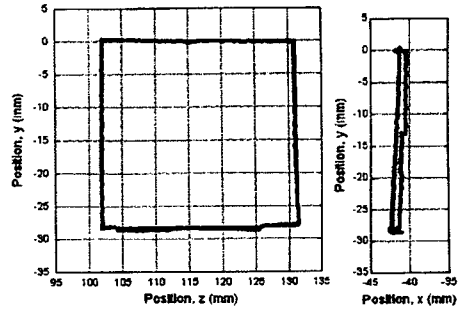

(e) Marker5

Fig. 8 Profile of five markers.

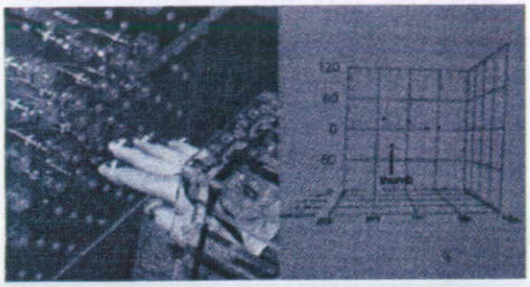

(a) Bending thumb

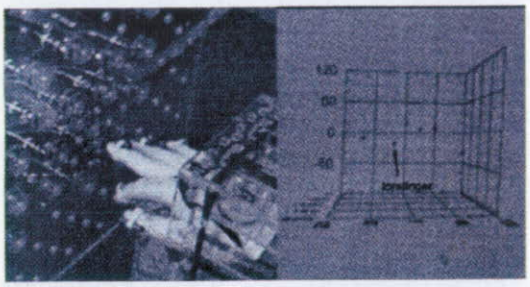

(b) Bending forefinger

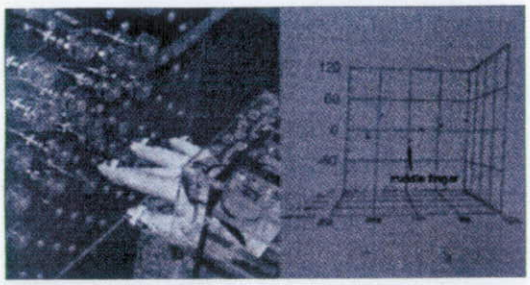

(c) Bending middle finger

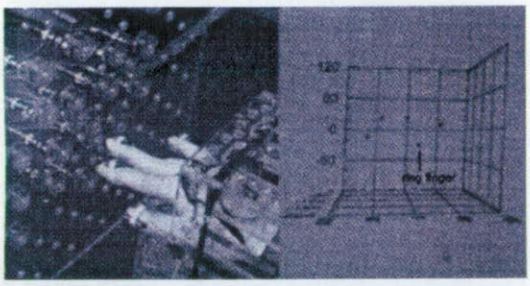

(d) Bending ring finger

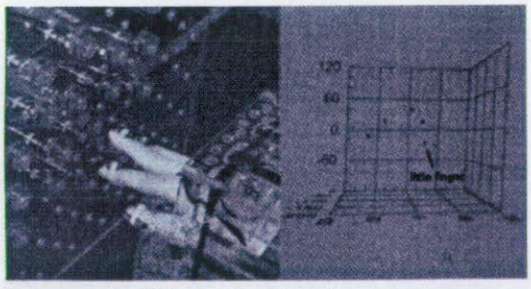

(e) Bending little finger

Fig. 9 Measured positions of fingertips.

なるように傾けた軌跡として求めた．yz 平面の軌跡では y 方向の変位量が 30mm よりも小さい値になっており，これは実際の磁気マーカの軌跡が x 軸方向へ若干傾いているためと考えられる．5 個のマーカにおいて，システムから得られた位置は理論的な軌跡とほぼ一致し，5 個のマーカの位置は同時かつ正確に計測できていることが了解される．

Table 2 はそれぞれマーカの位置精度を示したものである．位置精度は xy 平面および yz 平面において実測された軌跡と理論的な軌跡の最大の誤差を求め，全体の位置精度は xy 平面の精度と yz 平面の精度の相乗平均から算出した．Fig. 8 における一辺 30mm の正方形の移動距離において，相対位置精度は 1.1mm 以内であった．誤差要因としてはマーカが相互に接近しているために相互インダクタンスが共振周波数のずれとして計測され[2]，それが位置精度を悪化させているものと考えられる．

4.2 指先のモーションキャプチャ

Fig. 9 は各指先に貼付したマーカの写真および各マーカの位置を表示した動画の一部を静止画として表示したものである．各マーカの表示は Fig. 5 の z 軸の負方向から xy 平面を見る向きとした．5 個のマーカは手袋をはめた状態で各指の先端付近に貼り付けた．親指から順番に 1 本ずつ曲げる動作を繰り返した．(a) は親指のみを曲げた状態，(b) (c) (d) (e) はそれぞれ人差し指，中指，薬指，小指のみを曲げた状態をあらわしている．システムで得られた 5 個のマーカの位置はそれぞれの右側に点で表示されている．指先の位置は正確に計測されていることが了解される．計測速度は 20 Hz であり，指の通常の動きはほぼリアルタイムで計測可能であった．

5. まとめ

1. 5 個の共振型磁気マーカの位置検出システムを開発した．
2. 指先の運動範囲を想定した 30mm × 30mm の正方形の各辺において 5 個同時にマーカを移動させた場合の位置精度は 1.1mm 以内であった．
3. 指先にマーカを貼付して，リアルタイムに指先の位置を計測できるモーションキャプチャシステムを開発した．最高 20Hz で指先の動きを計測できた．

謝辞

PXI 計測システムの作製にご協力いただいた株式会社 CPI テクノロジーズ 高野卓雄氏，高野卓大氏，鎌田 勇氏に感謝いたします．本研究の一部は総務省の「戦略的情報通信研究開発推進制度」(5E5 番 126 号) の助成により行った．

References

1)http://www.solidray.co.jp/product/hanryoku/index.html.

2)http://www.nihonbinary.co.jp/Virtual/5DT/index.htm.
3)H. Sasaki, T. Kuroda, Y. Manabe, and K. Chihara, *Journal of the Virtual Reality Society of Japan*, vol. **7**, pp. 393-402 (2002).
4)J.A. Paradiso, K. Hsiao, J. Stricken, J. Lifton, A. Adler, *IBM Systems Journal,* vol. **39**, No. 3&4, pp. 892-914 (2000).
5) S. Yabukami, S. Hashi, Y. Tokunaga, T. Kohno, K.I. Arai, and Y. Okazaki, *Journal of the Magnetics Society of Japan,* vol. **28**, pp. 877-885 (2004).
6) S. Yabukami, T. Katoh, S. Hashi, K.I. Arai, and Y. Okazaki, *Journal of the Magnetics Society of Japan,* vol. **30**, pp. 218-224 (2006).
7) J.E. Mcfee, Y. Das, *IEEE Trans. Antennas and Propagation*, vol. **AP-29**, pp. 282-287(1981).
8) Nakagawa, Y. Koyanagi, Experimental Data Analysis by the least square method ,p.95-99, The University of Tokyo Press (1982).
9)S. Hashi, Y. Toyoda, S. Yabukami, K. Ishiyama, Y. Okazaki, and K. I. Arai, *IEEE Transactions on Magnetics*, vol. 43, pp. 2364-2366 (2007).

2007年5月10日受理, 2007年9月11日採録